Design of an ISFET Readout Circuit with Minimum Temperature Drift and Good Linearity

Abdelkhalak Harrak and Salah Eddine Naimi

Abstract Several researches are made on the readout circuit of the pH-ISFET, but, there is not much choice of readout circuit design. We will present in this article Caprio's quad-based readout circuit that minimize the temperature sensitivity and discuss several choices of geometry in the respect of saturation transistors. A Spice description as well as Veriloge-a were used to simulate the circuit using HSpice. The simulation was carried out in the temperature range from 20 °C to 80 °C, in the pH measurement range from 1 to 12 and with a supply voltage of ±3V. The proposed readout circuit was simulated in a CMOS 0.6 µm process. The circuit has very good performance in terms of temperature sensitivity and output linearity. Given the temperature change from 20 °C to 80 °C, the maximum temperature coefficient is 269.79 ppm/°C.

Keywords Ion-sensitive FET (ISFET) · Readout circuit · Chemical sensors · Temperature sensitivity

1 Introduction

In recent years, a great deal of research in the field of chemical and biological sensors entails solid-state sensors [1]. These research were stimulated by increasingly stringent requirements in the field of environmental quality control and biomedical analysis [2]. These include improved sensor sensitivity, response time and processing speed of the measurement data. Perfectly, we should be able to quickly and selectively detect any type of substance in the environment that we want to treat, with sensitivity up to a single molecule or ion. Different areas are very interested by an ISFET type sensor, since these sensors are more direct, faster, more accurate, more selective and cost less than other methods of analysis. In addition, because

A. Harrak (✉) · S. E. Naimi
SDMN Team, ERSETI Laboratory, ENSA, Mohammed First University,
BP 669, 60000 Oujda, Morocco
e-mail: a.harrak@ump.ac.ma

S. E. Naimi
e-mail: s.naimi@ump.ac.ma

B. Hajji et al. (eds.), *Proceedings of the 2nd International Conference on Electronic Engineering and Renewable Energy Systems*, Lecture Notes in Electrical Engineering 681, https://doi.org/10.1007/978-981-15-6259-4_41

of their small size, high sensitivity, and ability to integrate them on a chip, ISFET-based sensors are good candidates for meeting these requirements. These derivatives are not limited to chemical sensors, but also to biochemical sensors [3]. One of the most popular is EnFET (Enzymatic Field Effect Transistor), which is an enzymatic sensor [4]. An enzymatic layer covers the sensitive area and allows the detection of biochemical molecules such as urea, creatinine, glucose, triglyceride and lactic acid [5, 6]. Still based on FET technology, BioFETs allow biological detection [7, 9], such as ImmunoFET which opens the way of immunodetection [8], or the DNAFET which allows the analysis of DNA structures [9]. These sensors based on field effect transistors benefit from the development and technological progress, in particular microelectronics, which allows miniaturization and mass production, and thus low-cost components. In addition, they do not require specific packaging and are not fragile as the glass electrodes. The operation of the ISFET is that of the conventional MOS transistor, where the metal gate is replaced by the electrolyte biased by a reference electrode. Today, the current needs remain:

- Low temperature sensitivity for better measurement accuracy;
- A better passivation, due to the total impermeability between the aqueous medium and the electrical contacts;
- The integrated electrode, the integration of the electrode will allow portability, size and reduced costs of the detection system;
- The sensitive layer, to have more selective sensors, less sensitive to the elements interfering;
- Data processing, because it is necessary to develop a practical instrumentation and low cost;
- Modeling, because for the implementation of models faithfully reflecting reality, we must optimize any component. These models will help understanding physical phenomena and the evaluation of their impact on detection. So the reproducibility and detection parameters (sensitivity, detection range ...) will be improved.

In this article, we will present a readout circuit composed of a Caprio's quad fed by a current source simulated in HSpice and composed on the other hand of two models modeled in Veriloge-a which are two attenuators and a differential amplifier. We will also present a mathematical module which checks the saturation of the transistors that make up the Caprio's quad circuit which leads to a relationship between the widths of the channels of their transistors, the more a relationship has been established between the output currents and the dimensions of the transistors current mirror.

2 Design of the Readout Circuit Blocks

2.1 ISFET Structure

The ISFET transistor resembles the MOSFET transistor, the only difference between them is that the metal gate of the MOSFET has been replaced by a poly-crystalline

silicon gate and connected to the passivation layer through appropriate intermediate metal layers and vias. As shown in Fig. 1, the solution is polarized by a reference electrode, the solution also in direct contact with the silicon nitride passivation layer, which acts as a membrane sensitive to hydrogen ions. This nitride membrane is a good candidate for the detection of hydrogen ions in the electrolyte, a variation of the concentration of H+ ions in a solution causes a variation of the pH, which varies the drain-source current of the sensor. The difference between the concentration of the charge in the solution and the dielectric surface creates a potential:

$$\psi_0 = \frac{q}{C_{eq}}\left[N_{sil}\left(\frac{exp(\frac{-2\psi_0}{U_T})-exp(log(k_a\times k_b)+4.6\text{pH})}{exp(\frac{-2\psi_0}{U_T})+exp(log(k_a)+2.3\text{pH})exp(\frac{-\psi_0}{U_T})+\exp(\log(k_a\times k_b)+4.6\text{pH})}\right) + qN_{nit}\left(\frac{exp(\frac{-\psi_0}{U_T})}{exp(\frac{-\psi_0}{U_T})+\frac{K_n}{K_a}exp(log(k_a)+2.3\text{pH})}\right)\right] \quad (1)$$

With,

$$C_{eq} = \frac{C_{Gouy}C_{Helm}}{(C_{Gouy}+C_{Helm})} \quad (2)$$

Where, N_{sil} is the density of silanol sites, N_{nit} the density of amine sites. U_T the thermal voltage, k_a, k_b and k_n are the dissociation constants of the chemical reactions at the insulator interface. The capacitances C_{Gouy} and C_{Helm} are related to the Gouy-Chapman-Stern double-layer model. The flat band voltage is expressed as follows:

$$\Delta V_{FB} = V4 - V5 \quad (3)$$

Also, (3) it can rewrite as follows:

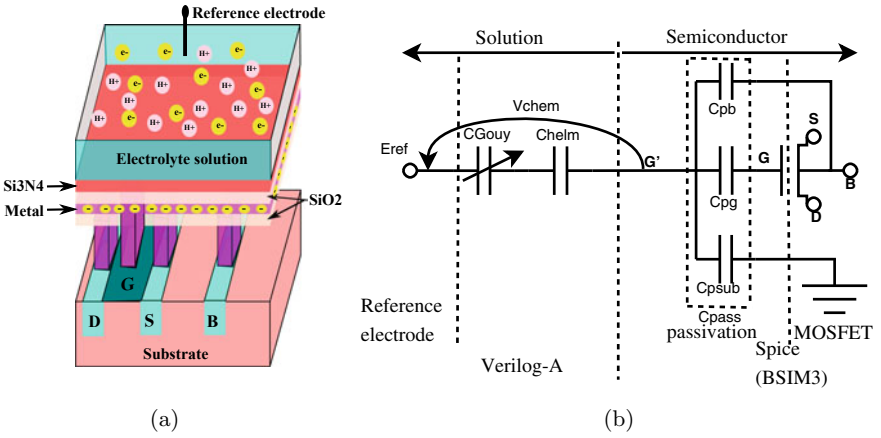

Fig. 1 **a** 3-D Cross-sectional illustration through a pH-sensitive ISFET with a floating gate electrode, **b** Small signal macro model circuit of the ISFET in solution

$$\Delta V_{FB} = E_{ref}(\frac{A_g}{A_{gCl}}) - 298.16\frac{dE_{ref}}{dT} + E_{abs} + \chi^{sol} + \Delta\varphi^{lj} - \frac{Q_{ig}}{C_{ig}} \\ -T[2.303\frac{K}{q}S(pH_{pzc} - pH) - \frac{dE_{ref}}{dT}] \quad (4)$$

Where, T is the system temperature, K the constant of Boltzmann, q the charge, pH_{pzc} a non zero pH, S the factor of sensitivity of the gate insulating, $E_{ref}(A_g/A_{gCl})$ the potential of the reference electrode is independent of the temperature, E_{abs} is the normalized potential of hydrogen, $\Delta\varphi^{lj}$ the potential drop between the solution and the reference electrode, χ^{sol} the dipole potential of the surface electrolyte-insulator and the complementary term Q_{ig}/C_{ig} represents the contribution of the trapped charge in the intermediate gate in the CMOS process.

2.2 The Readout Circuit

The readout circuit becomes essential to compose pH sensors based on the ISFET. The standard CMOS process can be used to integrate the pH-ISFET with a readout circuit to improve their performances [10, 11].
In this article, we propose a new approach in the design of the readout circuit, as can be seen in Fig. 2; the proposed circuit is composed of four blocks:

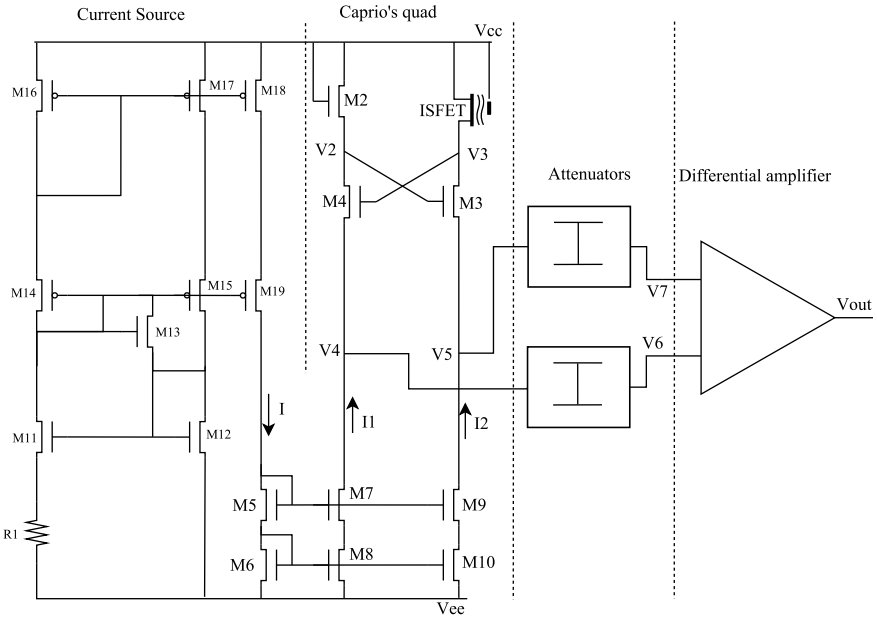

Fig. 2 The proposed readout circuit approach

– The first block is a modified current source, used to feed the circuit via the current mirror, its output is connected to the input of the cascode current mirror, and the latter shares the current with other blocks of the circuit. The Ohmic component R1 play the role of an voltage current converter, so the current reference can be generated from the voltage reference by using R1.
– The second block is a Caprio's quad used to extract flat band variation ΔV_{FB} generated by the concentration of the charges in the electrolyte. The difference in voltage appears at the output of the block between V4 and V5.
– The third block is composed of two attenuators used to modify the signals V4 and V5 to be adapted to the linear region of the differential amplifier, these two attenuators are modeled in Verilog-a and implemented in HSpice. The model of attenuator that we implemented is as shown in (5) and (6).

$$V6 = \alpha_1 V4 - \alpha_1' \tag{5}$$

And

$$V7 = \alpha_2 V5 - \alpha_2' \tag{6}$$

Where, V4 and V5 are the inputs of the attenuators, V6 and V7 are the attenuator's outputs, α_1 and α_2 are the attenuation coefficients, these coefficients are optimized in HSpice, α_1' and α_2' are the offset constants of the attenuators.
– The fourth block is a differential amplifier used to divide the voltage difference between V4 and V5 on the temperature; this amplifier is also modeled in Verilog-a and implemented in HSpice. The differential amplifier model is as follows:

$$V_{out} = \frac{(V6 - V7)}{T} \tag{7}$$

The purpose of the proposed readout circuit is to compensate the sensitivity to temperature and to provide better linearity of the signal in the output, for good measurement accuracy at a precise pH point. The readout circuit is designed to size the Caprio's quad, the current source and the current mirror simulated in MATLAB and HSpice, as the first part of the readout circuit, connecting this later with the second one, which consists of two attenuators and differential amplifier that is modeled in Verilog-a.

2.3 Saturation of the Caprio's Quad

The expressions of Eqs. (8), (9), (10) and (11) occur by the expression of current in the drain of a MOSFET transistor, in the region of saturation.

$$V_2 = V_1 - V_{TH0} - \sqrt{\frac{2L_2 I_1}{U_0 C_{ox} W_2}} \tag{8}$$

$$V_5 = V_2 + V_{TH0} - \sqrt{\frac{2L_3 I_2}{U_0 C_{ox} W_3}} \tag{9}$$

$$V_3 = V_1 - V_{TH0} - V_{pH} + \sqrt{\frac{2L_1 I_2}{U_0 C_{ox} W_1}} \tag{10}$$

$$V_4 = V_3 - V_{TH0} + \sqrt{\frac{2L_4 I_1}{U_0 C_{ox} W_4}} \tag{11}$$

By developing Eqs. (8), (9), (10) and (11) lead to the limit saturation conditions of the caprio's quad circuit (12).

$$C_1 \leq V_4 \text{ and } V_4 \leq C_2 \tag{12}$$

With C_1 and C_2 are given by (13) and (14)

$$C_1 = V_1 - 3V_{TH0} - \sqrt{\frac{2L_3 I_2}{U_0 C_{ox} W_3}} - \sqrt{\frac{2L_4 I_1}{U_0 C_{ox} W_4}} \tag{13}$$

$$C_2 = V_1 - V_{TH0} + \sqrt{\frac{2L_3 I_2}{U_0 C_{ox} W_3}} - \sqrt{\frac{2L_4 I_1}{U_0 C_{ox} W_4}} \tag{14}$$

Where U_0 is the electron mobility, C_{ox} is the capacitance of insulator, W is the channel width, L is the channel length and V_{TH0} is the threshold voltage. Caprio's quad circuit input currents play a very important role in improving the sensitivity of the circuit output to temperature and linearity, in other words, a random variation in current circuit dimensions can cause a large variation in sensitivity at temperature, also a deviation in linearity of the output, then to avoid these effects, the relation (15) must be respected, which varies proportionally with the geometry ratio α of the transistors (M5, M6, M7, M8, M9 and M10).

$$I_i = (\alpha + 0.5)\, I \pm \alpha\, \Delta I \text{ with } (i = 1 \text{ or } 2) \text{ and } \alpha = \frac{\mathrm{W}_{5,6}}{\mathrm{W}_{7,8}}, \frac{\mathrm{W}_{5,6}}{\mathrm{W}_{9,10}} \tag{15}$$

The current I_i can be I_1 or I_2 , measured in the transistor drain M7 and M9 respectively and I is the drain current of the transistor M5. W is the channel width, L is the channel length. The channel widths W of the four Caprio's quad transistors obey to the relation (16) and the length of the channel L is the same for all transistors.

$$W_1 = W_2 - 5 \text{ and } W_2 = W_3 = W_4 \tag{16}$$

3 The Simulation Results

3.1 Saturation of Caprio's Quad

Use of boundary conditions of the Eq. (14), the dimensions of the transistors W1, W2, W2 and W4, based on measured results, are calculated and illustrated in Fig. 3, the widths of the transistor channels react perfectly with relation (16), in fact, the three transistors M1, M2 and M3 have the same channel widths and are small than the channel width of M4 with a pitch of 5 μm, as shown by the labels above in Fig. 3. The Fig. 4 illustrates the input I and output currents I1 and I2 of the mirror current, as shown in the Fig. 4 the inputs and outputs do not change with the temperature variation, in other words the current mirror insensitive to temperature, not only that, but there is a relation between the entry of the current mirror and their exits, the exit currents change proportionally with a report of the geometry of their transistors and that proved by the relation in (15). The Fig. 5 on the left shows the boundary conditions of V4 to check the operation in the region of saturation of the transistors which make up the Caprio's quad, and Fig. 5 on the right presents V4 as a function of I1 and W4, to show the similarity with the results obtained in the Fig. 3.

3.2 The Readout Sensitivity and Linearity

In this section, we will see how the proposed readout circuit meets the desired objective; we simulate this readout circuit using the CMOS AMI 0.6 μm process provided by MOSIS. The results of the optimization of the readout circuit are shown in Fig. 6.

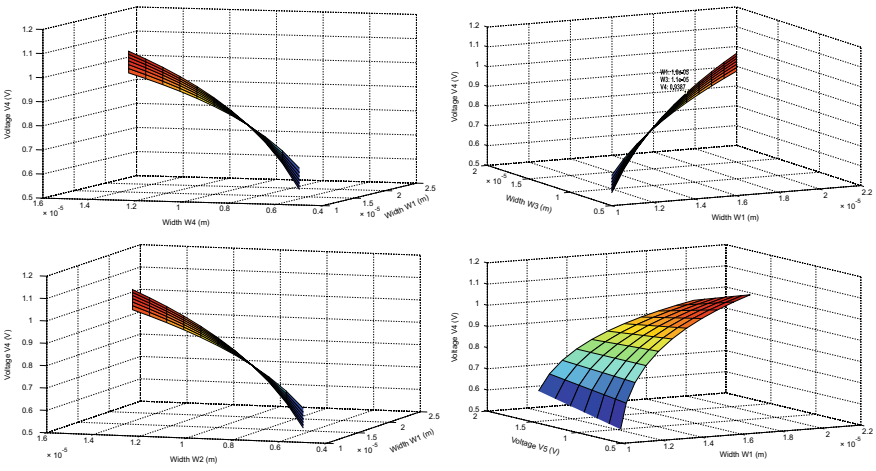

Fig. 3 Channel width fields that check saturation

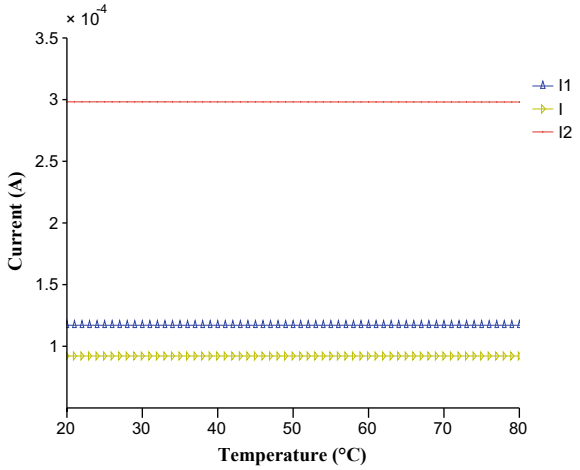

Fig. 4 The input and the output currents of the current mirror

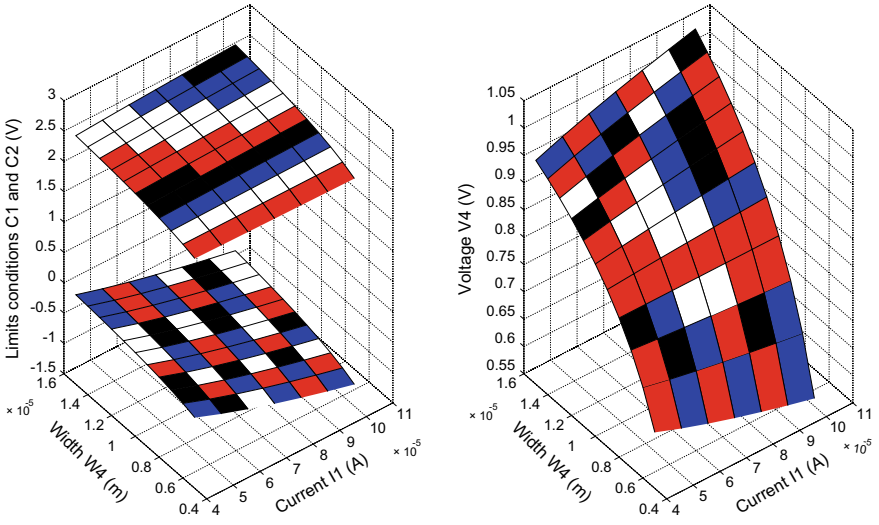

Fig. 5 the simulation of the boundary conditions of V4

As confirmed in the Fig. 6, the output signal is linear with the pH and the design methods allow better insensitivity to temperature. The two curves coincide in two different temperatures, the curve pointed at $T = 20\,^{\circ}\mathrm{C}$ and the straight curve at $T = 80\,^{\circ}\mathrm{C}$. Figure 6 shows the output of the proposed readout circuit sensor when the pH value changes from 1 to 12, the output gives a good linearity which is revealed by the coefficient of determination, $R^2 = 0.999986$ at $T = 20\,^{\circ}\mathrm{C}$ ($R^2 = 0.999985$ at $T = 80\,^{\circ}\mathrm{C}$).

The results claimed that the proposed circuit is a promising candidate for best linearity. This work also performs a temperature sweep of 20 °C to 80 °C in accordance

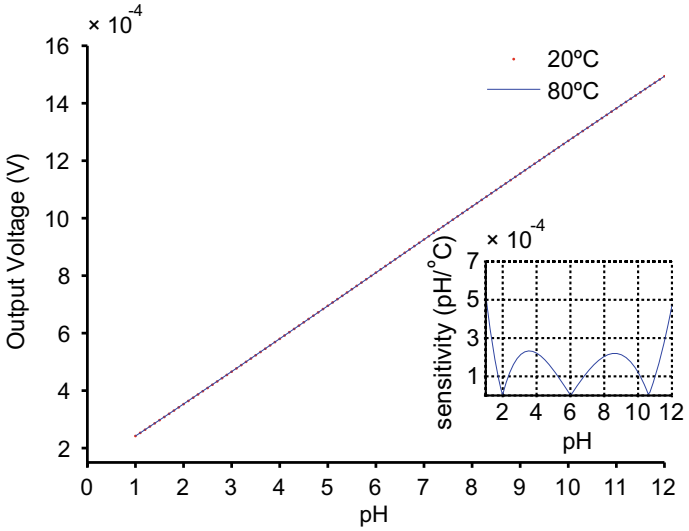

Fig. 6 The simulation of the output as a function of pH for the temperature 20 °C and 80 °C. In the right low corner: the calculated sensitivity of the output (pH/°C) versus the pH.

Table 1 Devices parameters list (channel length equal to 0.6 μm for all devices)

Device	W(μm)	Device	W(μm)
ISFET	15	M11	3
M2	10	M12	12
M3	10	M13	9
M4	10	M14	27
M5	4	M15	3
M6	3	M16	166
M7	7	M17	3
M8	7	M18	30
M9	3	M19	3
M10	3		

with a pH change of 1 to 12. The temperature compensation results are shown in the right low corner of the Fig. 6, as indicated, the maximum temperature sensitivity is 0.00052 pH/°C for a value of pH = 1 and the sensitivity less than 0.0002631pH/°C between pH = 1.4 and pH = 11.4, indeed the sensitivity value 0.0001616pH/°C is for pH = 7.4, the pH corresponding of human blood and the sensitivity is only equal 2.37×10^{-6} pH/°C for pH = 6.

The transistors sizes are presented in the Table 1 above, the current source resistor R1 was optimized and its value is around 300 KΩ. For the attenuators, their attenuation coefficients are 0.9 and 0.9009 respectively.

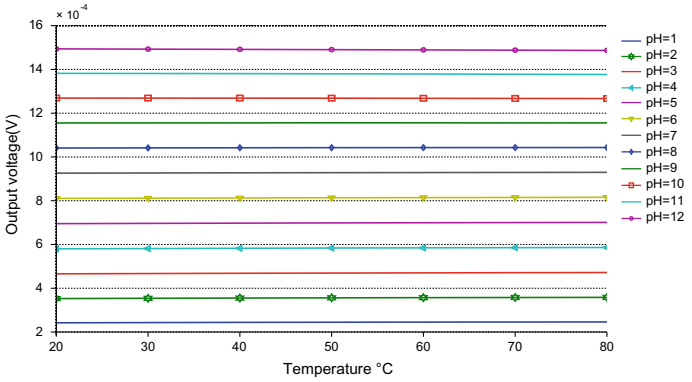

Fig. 7 Temperature variations of the output measurement

Table 2 Temperature coefficient TC (ppm/°C) of different pH values

pH	TC	Vout(10^{-4}V)	pH	TC	Vout(10^{-4}V)
1	269.79	2.44	7	68.57	9.28
2	252.88	3.65	8	36.83	10.43
3	212.89	4.70	9	9.99	11.65
4	172.63	5.83	10	28.71	12.69
5	135.41	6.98	11	63.28	13.80
6	101.06	8.13	12	79.69	14.91

3.3 Temperature Coefficient (TC)

Figure 7 shows the readout output trend with temperature at different pH values. We can appreciate the good temperature compensation obtained in the range of 20 °C to 80 °C for different pH. From the Vout-T curves, we can calculate the TC as follows:

$$TC(\text{ppm}/^{\circ}\text{C}) = \frac{(V_{outmax} - V_{outmin})}{(V_{outmean}(T_{max} - T_{min}))} 10^6 \tag{17}$$

Where V_{outmax} and V_{outmin} are the maximum and the minimum values of V_{out} in the considered T range respectively, and $V_{outmean}$is their mean value. The calculated TC ranges from 269.79 ppm/°C at pH = 1 down to 9.99 ppm/°C at pH = 9. The readout circuit reduces the temperature coefficient, as illustrated in the Fig. 7, the deviation of the output voltage as a function of the temperature is very small, and this is also illustrated by the results of the temperature coefficient in the Table 2.

The maximum temperature coefficient is 269.79 ppm/°C for a pH = 1, on the other hand the minimum temperature coefficient only 9.99 ppm/°C for a pH = 9, moreover the proposed circuit is a good candidate for the measurement of the pH of

human blood, knowing that human blood has an alkaline pH between 7.3 and 7.4, corresponding with the temperature coefficient between 68.57 and 36.83 ppm/°C.

4 Conclusion

In this study, the Verilog-a language, have been used to describe the behavior of the electrode-electrolyte-sensitive membrane structure of the pH-ISFET. While a standard model (BSIM3v3) was used in conjunction with HSpice for the MOSFET part of the sensor. The 0.6 μm CMOS technology from AMI was used to simulate the proposed circuit. The readout circuit gives good results for a temperature range between 20 °C and 80 °C and a wide pH range between 1 and 12. The temperature sensitivity of the circuit is less than 0.00052 pH/°C and also gives good linearity attend at 99.99, the proposed circuit is a good candidate for the measurement of the pH of human blood, knowing that human blood has an alkaline pH of between 7.3 and 7.4, the temperature coefficient which is less than 68 ppm/°C.

Appendix

Model Verilog-a of the attenuators

```
module attenuateur(in1,in2,in3,in4,out1,out2);
input in1,in2,in3,in4;
inout out1,out2;
electrical in1,in2,in3,in4,out1,out2;
analog begin
V(out1,out2) <+ V(in3,in4)*V(in1,in2);
end
endmodule
```

Model Verilog-a of the differential amplifier

```
module diviseur(in1,in2,in3,in4,out1,out2);
parameter Delta=0;
input in1,in2,in3,in4;
inout out1,out2;
electrical in1,in2,in3,in4,out1,out2;
analog begin
V(out1,out2) <+ (V(in3,in4)-V(in1,in2))/(temperature + Delta);
end
endmodule
```

References

1. Steinhoff G, Hermann M, Schaff WJ, Eastman LF, Stutzmann M, Eickhoff M (2003) pH response of GaN surfaces and its application for pHsensitive field-effect transistors. Appl Phys Lett 83:177–179. https://doi.org/10.1063/1.1589188
2. Jiang Y, Coquet P, Yu H (2018). Fast food safety screening with CMOS high sensitivity large-arrayed ISFET sensor. In: Proceedings of the IEEE biomedical circuits and system, BioCAS 2017 , 1–4 January 2018. https://doi.org/10.1109/BIOCAS.2017.8325174
3. Kalofonou M, Toumazou C (2014) A low power sub- μ w chemical gilbert cell for isfet differential reaction monitoring. IEEE Trans Biomed Circuits Syst 8:565–574. https://doi.org/10.1109/TBCAS.2013.2282894
4. Sant W, Temple-Boyer P, Chanié E, Launay J, Martinez A (2011) On-line monitoring of urea using enzymatic field effect transistors. Sensors Actuators B Chem 160:59–64. https://doi.org/10.1016/J.SNB.2011.07.012
5. Zhao S, Shi C, Hu H, Li Z, Xiao G, Yang Q, Sun P, Cheng L, Niu W, Bi J, Yue Z (2020) ISFET and Dex-AgNPs based portable sensor for reusable and real-time determinations of concanavalin A and glucose on smartphone. Biosens Bioelectron 151:111962. https://doi.org/10.1016/j.bios.2019.111962
6. Kaisti M (2017) Detection principles of biological and chemical FET sensors. Biosens Bioelectron 98:437–448. https://doi.org/10.1016/j.bios.2017.07.010
7. Vacic A, Criscione JM, Stern E, Rajan NK, Fahmy T, Reed MA (2011) Multiplexed SOI BioFETs. Biosens Bioelectron 28:239–242. https://doi.org/10.1016/J.BIOS.2011.07.025
8. Juang DS, Lin CH, Huo YR, Tang CY, Cheng CR, Wu HS, Huang SF, Kalnitsky A, Lin CC (2018) Proton-ELISA: Electrochemical immunoassay on a dual-gated ISFET array. Biosens Bioelectron 117:175–182. https://doi.org/10.1016/j.bios.2018.06.012
9. Kalofonou M, Georgiou P, Ou CP, Toumazou C (2012) An ISFET based translinear sensor for DNA methylation detection. Sensors Actuators B Chem. https://doi.org/10.1016/j.snb.2011.09.089
10. Oldham KB (2008) A Gouy-Chapman-Stern model of the double layer at a (metal)/(ionic liquid) interface. J Electroanal Chem 613:131–138. https://doi.org/10.1016/J.JELECHEM.2007.10.017
11. Cong Y, Xu M, Zhao D, Wu D (2017). A 3600 x 3600 Large - scale ISFET Sensor Array for High - throughput pH Sensing, pp 957–960